THE JOURNAL OF PHYSICAL CHEMISTRY Letters

Letter

pubs.acs.org/JPCL

Effect of Packing on Formation of Deep Carrier Traps in Amorphous Conjugated Polymers

Svetlana Kilina,[†] Naveen Dandu,[†] Enrique R. Batista,[‡] Avadh Saxena,[‡] Richard L. Martin,[‡] Darryl L. Smith,[‡] and Sergei Tretiak*[,‡,§]

[†]Department of Chemistry and Biochemistry, North Dakota State University, Fargo, North Dakota 58108, United States

[‡]Theoretical Division and [§]Center for Integrated Nanotechnologies (CINT), Los Alamos National Laboratory, Los Alamos, New Mexico 87545, United States

Supporting Information

ABSTRACT: We theoretically investigate the role of conformational disorder and intermolecular interactions on the localization properties of electronic states, leading to the formation of carrier traps in amorphous aggregates of conjugated polymers. Samples of amorphous conformations of poly(*p*-phenylene vinylene) (PPV), poly2-methoxy-5-(2-ethyl-hexyloxy)PPV (MEH-PPV), and [poly-(9,9′-dioctyluorene)] (PFO) oligomers are simulated by classical molecular dynamics, while their electronic structure is calculated using first-principles density functional theory. Localization and delocalization properties of molecular orbitals are studied based on the participation ratio analysis, an approach commonly used in inorganic semiconductors. Our simulations confirm that the alkyl side chains insignificantly affect the conformational disorder in amorphous polymers while having a dramatic effect on the intermolecular disorder and packing. The nature of the disorder and its impact on charge-carrier localization in amorphous polymers with alkyl side chains differ drastically from those of disordered polymers without side chains, such as PPVs. Thus, long-range intermolecular interactions and sparse packing are responsible for the formation of multiple, deep, highly localized trap states in amorphous MEH-PPVs and PFOs, while close packing in combination with conformational disorder leads to the trap states distributed mostly near the bandgap edges in PPV aggregates.

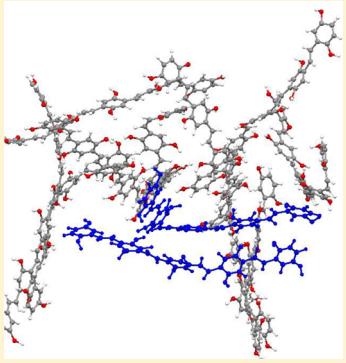

SECTION: Molecular Structure, Quantum Chemistry, and General Theory

Photoluminescent π-conjugated polymers (PCPs) are also called as organic semiconductors. The tunability of their color in light emission afforded via chemical synthesis, mechanical flexibility, solubility, and low-cost fabrication promises a number of technological advantages over the traditional semiconductors.[1−3] However, the "soft" structure of organic semiconductors results in a highly amorphous morphology. Strong variations in the PCP morphology, in turn, lead to vast differences in their photophysical and transport properties, which are challenging to control in such highly disordered materials.[4−7] Unlike inorganic semiconductors, disorder in the PCPs is not associated with broken chemical bonds. It has two general origins: Intramolecular conformations lead to variations in bond lengths, torsional angles, and the appearance of on-chain defects, whereas intermolecular interactions arise from material morphology, chain alignment, and packing. Each of these disorders might be responsible for carrier trapping, which decreases electronic transport and quenches luminescence in PCPs. The complexity involved in identifying a disorder type and, consequently, understanding the ways to control it in PCP materials poses high demands to both experimental and theoretical techniques.

In films, PCPs are typically self-organized into several distinct supramolecular structures, where crystalline domains are separated by less ordered or completely amorphous regions.[4,8] In the same PCP material, therefore, different concentrations of ordered and disordered domains result in various experimental values of hole/electron mobility,[9] while average values of charge carrier mobility are misleading.[10] It is well known that the carrier mobility is trap-limited in PCP materials, especially for electrons. Nevertheless, because of the microscopically heterogeneous morphology of PCP films, it is extremely challenging to experimentally define the exact origin of the traps in organic semiconductors.[11] As a result, little consensus exists in the literature regarding understanding of transport in PCPs. Efficient development of PCP-materials with enhanced transport properties, however, requires microscopic information on the relationship between structural and physical properties, from which scientists and engineers can optimize organic optoelectronic devices.

Theoretical analysis based on atomistic calculations can potentially offer such a physical picture, which includes the electronic structure, the morphology, the interplay between different types of disorder, and the effect of this interplay on the delocalization/localization of the electronic charge density and

Received: February 13, 2013
Accepted: April 7, 2013
Published: April 7, 2013

dx.doi.org/10.1021/jz4003197 | *J. Phys. Chem. Lett.* 2013, 4, 1453−1459

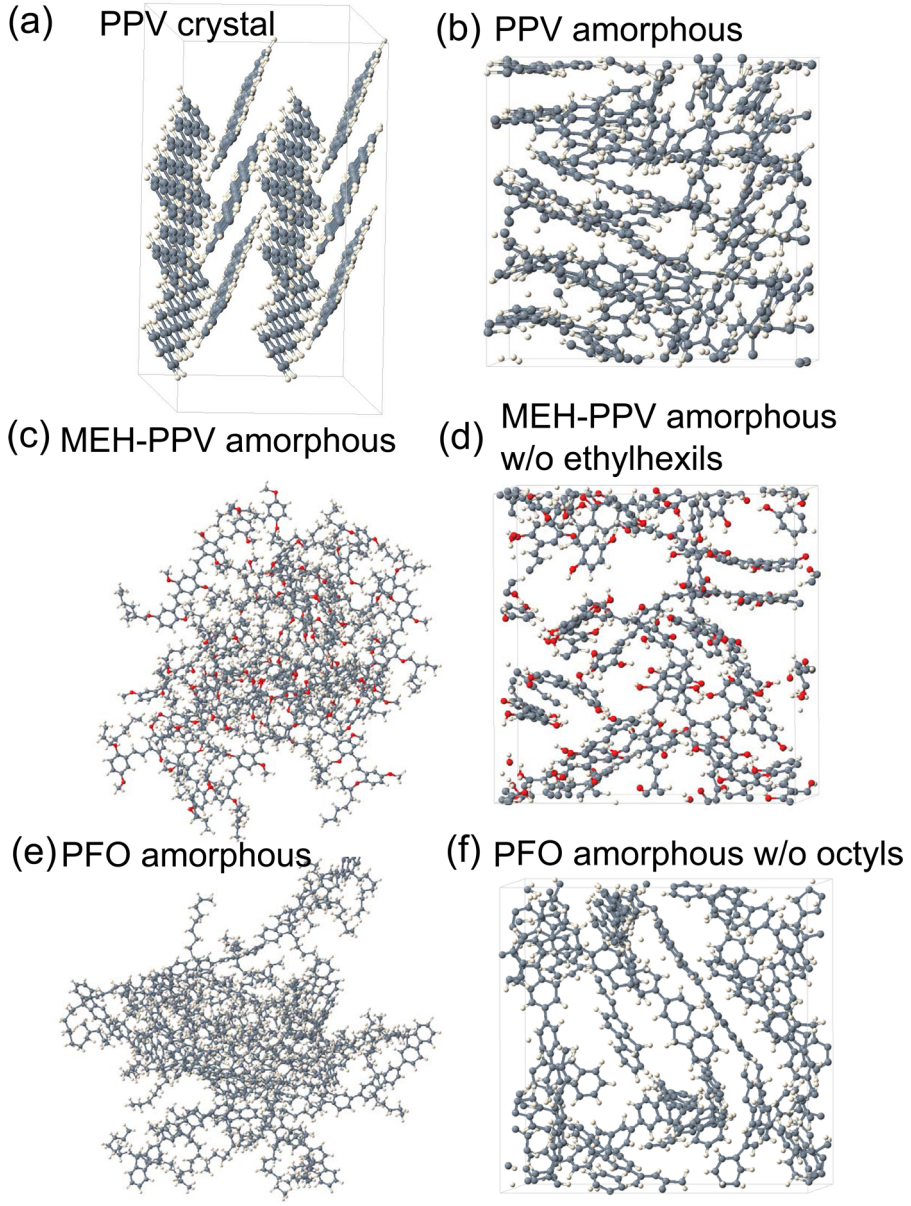

Figure 1. Representative snapshots of the MD-simulated structures of the PCP systems we studied. (a,b) Crystal and amorphous phase of the PPV cluster containing 12 pentamers in a periodically repeated simulation cell of ~3 × 3 × 3 nm^3 size. (c,d) Amorphous MEH-PPV aggregate with (left) and without (right) ethylhexil side chains. The simulation cell includes 12 MEH-PPV pentamers. (e,f) Amorphous PFO aggregate with (left) and without (right) octyl side chains. The simulation cell includes eight PFO pentamers. Polymer chains extending over the boundary of the periodic box are shown in two different ways: Panels c and e display such chains as imaginary replicas into the next periodic cell to preserve the visual continuity of molecules. Panels b, d, and f project such chains to the opposite side of the same simulation cell.

formation of trap states in PCP materials. However, in practice, modeling the detailed physics of PCP systems also presents a great challenge. The main reason is the computationally unmanageable number of atoms in realistic amorphous polymer systems. Thus, atomistic information on the amorphous morphology is not affordable by quantum chemistry calculations, such as density functional theory (DFT) and semiempirical methods. Therefore, most of existing quantum chemistry studies have been focused on characterizing optical and transport properties of isolated oligomers.[12−17] The quantum chemistry approaches for larger and more realistic PCP systems are restricted to small amorphous aggregates,[18−21] where samples of amorphous conformations are obtained by molecular dynamics (MD) using classical force field (FF) calculations, while the electronic structure is calculated by DFT using the FF geometries.

Here we adopt the same approach[18−20] to simulate and compare the electronic structure of small amorphous aggregates of widely explored PCP materials for lighting and energy applications, such as PPV [poly(*p*-phenylene vinylene)], its derivative MEH-PPV [poly2-methoxy-5-(2-ethyl-hexyloxy)-PPV], and PFO [poly-(9,9′-dioctylfluorene)]. The main goal of our calculations is determining the role of intermolecular interactions and conformational disorder on the formation of carrier's trap states in PCPs of different chemical compositions and structures. The formation of trap states in PCPs has several effects on device operation. First, traps enhance nonradiative recombination processes, which decrease luminescence effi-

dx.doi.org/10.1021/jz4003197 | *J. Phys. Chem. Lett.* 2013, 4, 1453−1459

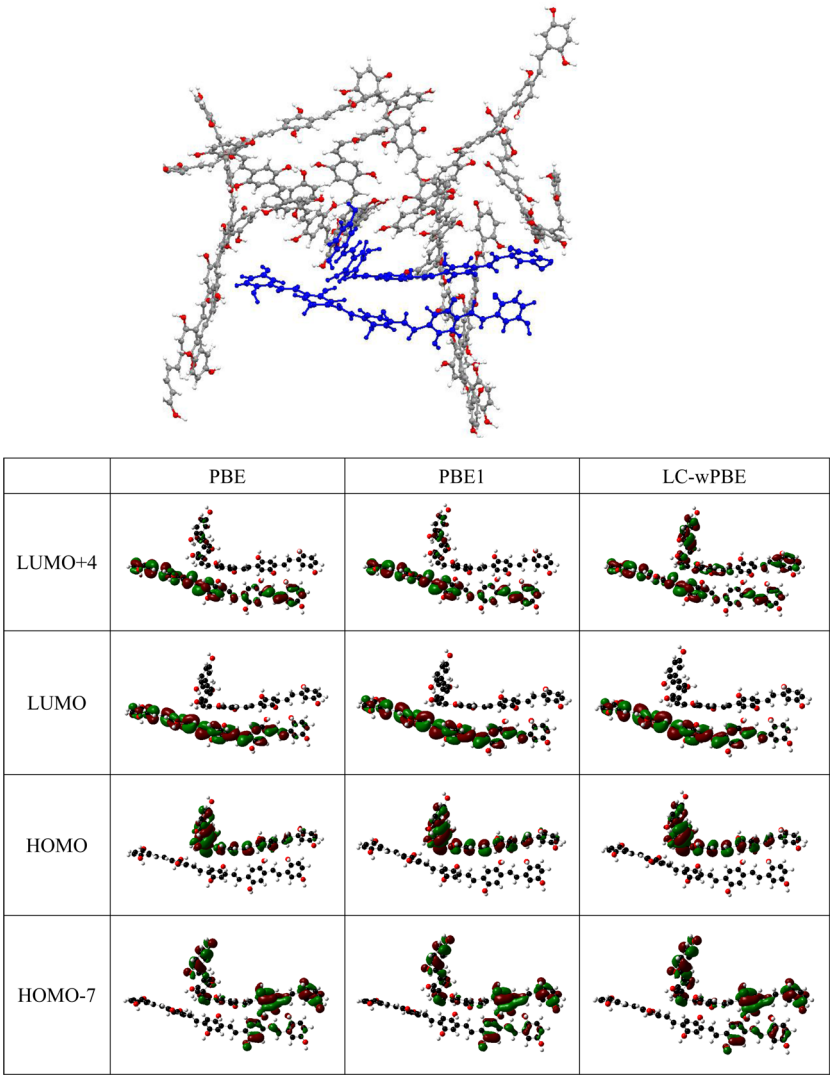

Figure 2. Selected MEH-PPV amorphous structure with the two marked oligomers used for calculations of molecular orbitals using PBE, PBE1, and LC-ωPBE functionals combined with 6-31G* basis set, as incorporated into the Gaussian 09 software package. Selected occupied and unoccupied molecular orbitals clearly show similar character of localization/delocalization properties of electronic states independent of the functional used.

ciency in organic light-emitting diodes (OLEDs), especially, at low voltages.[22,23] Furthermore, a trap-limited low electron mobility facilitates the formation of excitons close to the cathode and results in an energy transfer from PCP to the metallic leads, followed by nonradiative decay and material degradation.[24] Therefore, the determination of the energetic distribution of trap states and the mechanisms of their formation are of vital importance for controlling electrical properties of the PCP materials to understand and to optimize charge transport in PCP-based devices.[25]

Targeting this goal, we use a DFT-parametrized[18,19] MM3-2000 force-field potential to provide reliable geometries and packing morphologies for disordered polymer chains of PPV, MEH-PPV, and PFO. From 16 to 20 statistically probable samples of molecular geometries for the disordered PPV, MEH-PPV, and PFO pentamers (chains with repeating five-units) were generated by simulated annealing using periodic-boundary-condition (PBC) MD, as implemented in Tinker software,[26] following our previously developed methodology.[18,19] The MD-obtained amorphous aggregates with densities close to the experimental ones of ~1.25 g/mL (12 oligomers of PPV), 1.01 g/mL (12 oligomers of MEH-PPV), and 1.04 g/mL (8 oligomers of PFO) have been rapidly cooled from 2000 to 0 K, keeping the volume of the simulation cell unchanged.

Figure 1b–d shows an example of an amorphous aggregate of each PCP system we obtained from MD simulations. Because the alkyl side chains play a key role in the polymer packing determining the spatial distance between chains, side groups of MEH-PPV and PFO are preserved during the MD simulations of the amorphous aggregates. In the case of MEH-PPV and PFO disordered clusters, the total number of atoms in the computational cell is close to 3000, which is manageable for FF simulations but is problematic for DFT calculations. To reduce the number of atoms in the cell, while preserving the main physical properties of the system, the side chains (octyl groups in PFOs and ethylhexil groups in MEH-PPVs) have been replaced by hydrogens and methyl groups, while the MD geometry of the main polymer backbone is not changed. This reduced the number of atoms to about 800, as illustrated in Figure 1d,f, allowing for DFT electronic structure calculations. As can be seen from Figure 1d,f, the intermolecular spacing

dx.doi.org/10.1021/jz4003197 | J. Phys. Chem. Lett. 2013, 4, 1453–1459

between MEH-PPV and PFO chains is relatively large; the averaged smallest distance between carbon-rings in the neighboring chains is around 3.6 to 3.7 Å. This presumes relatively weak $\pi-\pi$ interactions between nearest chains compared with PPV amorphous aggregates, shown in Figure 1b, where the average smallest intermolecular distance is calculated to be ~3.3 Å (a typical van der Waals distance).

The subsequent electronic structure calculations of the disordered aggregates with reduced side groups and the crystal structure of the ordered PPV oligomers[18] (the structure is shown in Figure 1a) have been performed with the VASP code.[27] This code utilizes PBC DFT using a plane-wave basis set. The core electrons are simulated using the Vanderbilt pseudopotentials,[28] whereas all valence electrons are treated explicitly. The generalized gradient approximation (GGA) functional due to Perdew and Wang (PW91)[29] was used to account for the electron exchange and correlation effects. Because of the large size of the simulation cells (about 30 Å on each side), a Γ-point sampling of the Brillouin zone was adequate, as was shown in our previous work.[18,19] The effect of alkyl groups on the electronic structure of PFOs and MEH-PPVs was estimated by comparison of the electronic energies of the isolated pentamers with and without side groups. Electronic energies of both molecules coincided with an accuracy up to the third decimal place, proving a negligible impact of side chains on the electronic structure of the PFOs and MEH-PPVs.

Use of the GGA functional leads to underestimated energy gap values as compared with experimental PCP systems. This failure is typical for nonhybrid DFT calculations, stemming ultimately from the incomplete elimination of self-interaction by these functionals.[16] Comparison of the electronic structure for one of the MEH-PPV amorphous samples calculated using the standard GGA PBE model, the hybrid PBE1 functional (25% of Hartree−Fock (HF) exchange), and the long-range corrected LC-ωPBE kernel demonstrates a very similar profile of density of states (DOS) with an exception of increasing the band gap energy with the portion of the HF exchange in the functional, as discussed in the Supporting Information. These trends are well seen for the isolated molecules with exactly the same conformation they have in the amorphous sample, as well as for the entire amorphous snapshot consisting of 12 MEH-PPV oligomers. (See Figures S1 and S2 in the Supporting Information.) However, we are primarily interested in relative energetics of the electronic states and not in absolute values of the energy gaps. Qualitatively, the GGA functional provides a reasonable electronic structure of PCPs: the MEH-PPV amorphous aggregates have the smallest band gap, which is slightly increased (by ~0.4 eV) in PPV aggregates, while PFO disordered clusters have almost twice the band gap, as can be seen in Figure 4. The relative values of the band gaps agree qualitatively with the typical emission of these polymers, which is in the red-orange spectral range in MEH-PPVs, yellow-green in PPVs, and dark-blue in PFOs.

Moreover, localization properties might be also affected by the density functional used.[14−16] To get insight into this question while preserving reasonable computational cost, we have performed calculations of only two isolated molecules with exactly the same confirmation that they have in the amorphous MEH-PPV sample, as illustrated in Figure 2. These calculations were performed using PBE, PBE1, and LC-ωPBE functionals combined with the 6-31G* basis sets as implemented into the Gaussian 09 software package.[30] Our calculations presented in Figure 2 and in Figure S3 of the Supporting Information confirm that delocalization properties are not noticeably affected by the functional used. Consequently, observed orbital localization properties are attributed to the presence of the large conformational disorder in the samples of amorphous polymeric materials considered here.

Quantitatively, localization properties of occupied and unoccupied electronic states − characterizing the trap states − are studied based on participation ratio (PR) and inverse participation ratio (IPR) analysis, an approach commonly used in inorganic semiconductors[31] first defined by Thouless, Dean, and Bell.[32,33] The IPR (or PR) is widely used in the solid-state physics as a measure of disorder and localization in a bulk crystal of a volume[34] (V) or in a discrete space[31] (N atoms). For an ideally localized state on a single atom, PR = 1/IPR = 1. For a wave function uniformly distributed over all N atoms, PR = 1/IPR = N. To be applied for PCPs, we define PR in a molecular basis as

$$\mathrm{PR}(i) = \frac{(\sum_n P_{in})^2}{\sum_n P_{in}^2} = \frac{1}{\sum_n P_{in}^2}$$

where P_{in} is a portion of the PR orbital i on the nth molecule. More details of the methodology used for PR calculations can be found elsewhere.[19] According to this formula, an electronic state of a PCP aggregate that is completely localized on a single chain has PR = 1, while the state delocalized over all N molecules in the cell has PR = N. Calculations of the PR for the ideally ordered PPV crystal clearly elucidate this concept, as shown in Figure 3.

DOS of the PPV crystal, shown in Figure 3, represent well-separated sub-bands, each including 12 states contributed from 12 PPV oligomers in the crystal cell. The intermolecular interaction with a dominant $\pi-\pi$ character splits the energies of these 12 states, resulting in a finite width (~0.4 eV) of the sub-

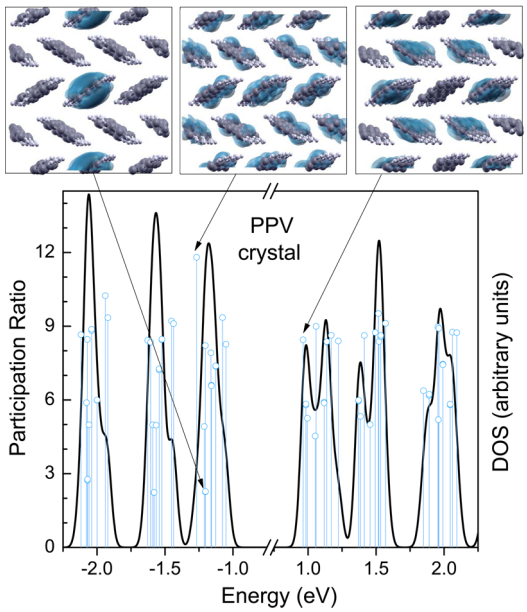

Figure 3. Calculated electronic structure of the ideal PPV crystal. Top panel shows the partial charge densities for selected electronic states. The bottom panel represents the density of states (DOS) and the participation ratio (PR). The calculated PR exactly correlates with a number of PPV oligomers that contribute to a particular electronic state.

dx.doi.org/10.1021/jz4003197 | J. Phys. Chem. Lett. 2013, 4, 1453−1459

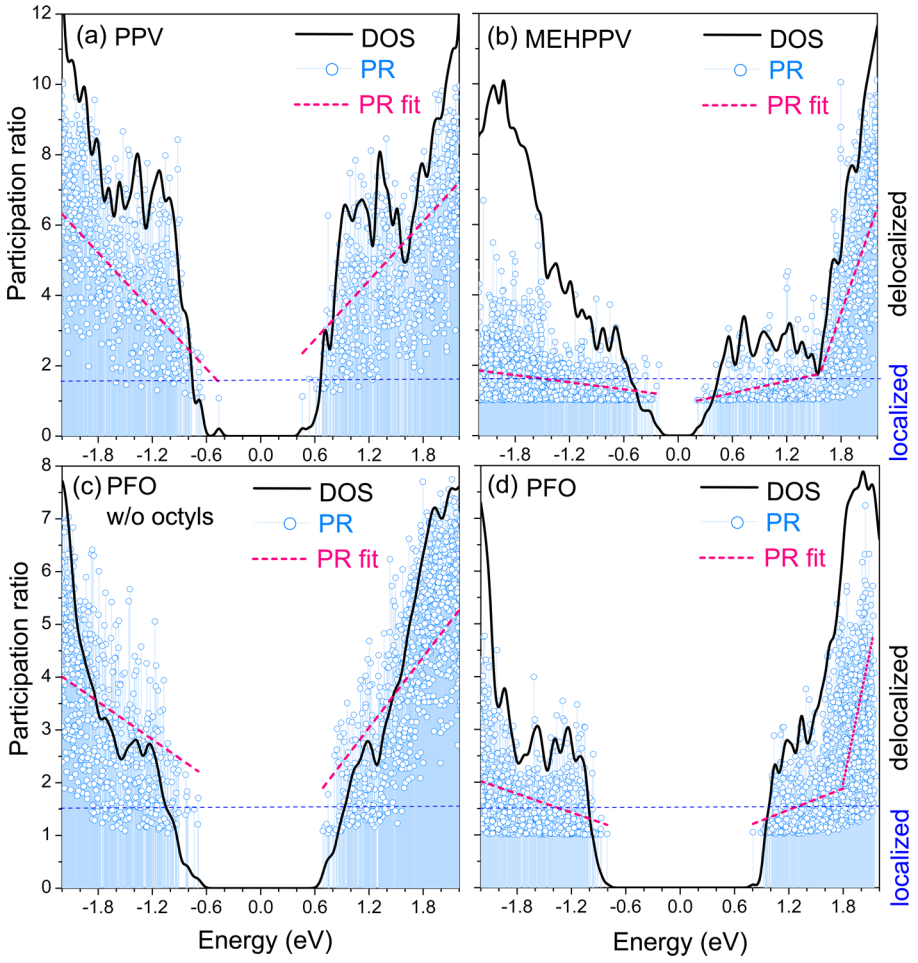

Figure 4. Calculated density of states (DOS) and participation ratios (PRs) representing averaged data for 16−20 different equilibrium configurations of amorphous aggregates: PPVs (a), MEH-PPV (b), modified PFOs with substituted octyl groups by hydrogens (c), and generic PFOs (d). The DOS values are shown in arbitrary units obtained by adding Gaussian broadening (of 0.02 eV) to the respective orbital energies. The PR distribution for each polymer is fitted to a linear dependence (dashed red lines). The smaller the PR, the stronger the localization of an electronic state. States with the PR < 2 correspond to trap states, orbitals that are highly localized on a single polymer chain. The substantial distinction in slopes of PR linear fitting between the left and right panels clearly shows that charge-carrier localization in amorphous PFOs and MEH-PPVs with long side chains drastically differs from those of polymers without side chains, such as PPV aggregates.

band. The intermolecular interactions are also reflected in the delocalized character of molecular orbitals, which are spread over several oligomers, or even over all molecules in the crystal cell, as shown in the top panel of Figure 3. The calculated PR exactly correlates with a number of PPV molecules that contribute to a particular electronic state. For example, the lowest unoccupied molecular orbital (LUMO) is delocalized over eight PPV molecules, as can be seen from the partial charge density of this state visualized in the top panel of Figure 3. Accordingly, the PR corresponding to the LUMO has a value of eight (vertical sticks in the bottom panel of Figure 3).

Figure 4 shows both DOS and PR as a function of energy for the combination of 16−20 different amorphous clusters of PPV, MEH-PPV, and PFO. In contrast with the PPV crystal, many electronic states of the amorphous PPVs, in particular, those that are close to the band edge, have a highly localized character with the PR < 2, as shown in Figure 4a. The intermolecular $\pi-\pi$ interactions in amorphous PPV aggregates are significant and comparable to the crystal PPV, as follows from the average intermolecular distance of 3.3 Å, which is typical for $\pi-\pi$ stacking. Therefore, it is mostly the intramolecular disorder in amorphous structures that results in strongly localized electronic trap states. In our previous work,[18] we disentangled the effects of intramolecular conformational disorder and the intermolecular interactions by comparing the entire system, which includes both intra- and intermolecular interactions, with the average of calculations of the isolated oligomers having the same geometry as those in the interacting, amorphous PPV cluster. This approach revealed that in amorphous PPVs electron trap states are favored by intramolecular configurational disorder, whereas hole trap states mostly resulted from intermolecular interactions,[18] confirmed by recent experimental studies.[8] In our current investigations on amorphous PPVs, we confirm this conclusion and clearly demonstrate that the electronic states near the band edge have a highly localized character, which makes them the carrier trapping states. Note that electronically highly localized trap states are about 0.6 to 0.8 eV below the energy of the first peak in the conduction band of the PPV crystal (compare DOS in Figure 4a and Figure 3). These values agree surprisingly well with recent experimental results from photothermal deflection spectroscopy and internal photoemission spectroscopy, confirming a Gaussian-shaped distribution of electronic traps centered 0.75 eV below the LUMO of PPV.[35]

dx.doi.org/10.1021/jz4003197 | J. Phys. Chem. Lett. 2013, 4, 1453−1459

The PR in Figure 4b,d clearly demonstrates the existence of numerous one-molecule-localized states not only close to the band gap edges but also deep in the valence band (VB) and conduction band (CB) in MEH-PPV and PFO aggregates. This localization behavior differs dramatically from that observed in amorphous PPVs as well as semiconductor disordered systems, such as hydrogenated amorphous silicon,[31] where only states near the energy gap are strongly localized while all other states in the bands show significant delocalization. Our results demonstrate that although the conventional band-like description is more or less appropriate for amorphous PPVs, it does not work for disordered MEH-PPVs and PFOs.

On first glance, such a strong difference in the electronic structure between amorphous PPV and its chemical derivative MEH-PPV as well as similarities between very different polymers such as MEH-PPV and PFOs seems surprising. The torsion angles between two nearest unit cells in the conjugated backbone of PPVs and MEH-PPVs significantly differ from PFOs: an isolated PPV or MEH-PPV chain has a planar geometry with the torsion angles close to 0° (or 180°),[36] while the ideal PFO molecule has a twisted geometry with torsion angles of 37° (or 143°).[12,37] Figure 5 displays a statistical analysis of the torsional angles in PFO, MEH-PPV, and PPV molecules calculated for the 16−20 different amorphous samples. Packing disorder has some effect on the optimal torsion angle in PCP systems, resulting in a broader distribution of torsion angles, which is most pronounced for PFO aggregates. A relatively high probability of PFO configurations with small torsional angles (0−60° and 120−180°) is a sign of substantial intermolecular interactions, allowing for optimal packing and π-stacking of the PFO chains.[19] Nonetheless, 40 and 140° remain the most probable values of the torsional angles in PFO aggregates, while 0 and 180° are the most probable torsion angles in PPV and MEH-PPV aggregates. Thus, neither intra- nor intermolecular disorder changes the similarities in torsion angles between MEH-PPV and PPV, which significantly distinguish these aggregates from PFOs. Because deep traps are not present in the DOS of amorphous PPV aggregates, which have similar torsion disorder as the MEH-PPV aggregates, the intramolecular disorder in torsion angles cannot be a reason for the appearance of highly localized trap states deep inside the VB and CB of amorphous MEH-PPVs and PFOs.

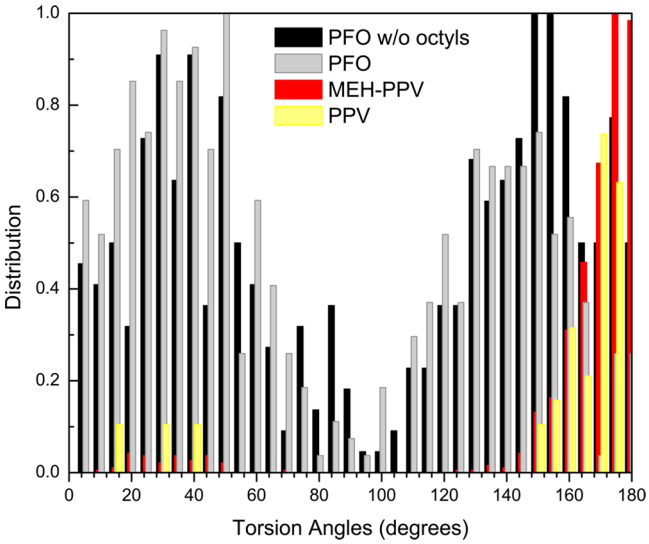

Figure 5. Comparison of torsional angle distribution between amorphous PPV, MEH-PPV, and PFO aggregates. All distributions are normalized and taken over 20 different amorphous samples of PFOs (black) and modified PFOs with substituted octyl groups by hydrogens (gray) and 16 amorphous samples of PPV (yellow) and MEH-PPV (red). Distribution of angles in amorphous PFOs is wider than that for PPV and MEH-PPV, pointing to stronger intramolecular conformational disorder in PFO aggregates. The presence of side chains negligibly changes torsion distributions; thus the side chains insignificantly affect the conformational disorder in PCP materials.

A distinct structural feature, which might be responsible for the difference in orbital localization, is the long alkyl side chains that are present in PFO and MEH-PPV aggregates and lacking in PPV structures. Such side chains hinder close packing between oligomers and increase the closest intermolecular distances in PFOs and MEH-PPVs (~3.6 to 3.7 Å) so that intermolecular interactions are reduced compared with the amorphous PPVs without side chains. To create a complete analogy between PPV and PFO aggregates, we have modeled amorphous clusters of modified PFO molecules that are lacking the octyl side groups from the very beginning of the MD simulations. The absence of the side groups in such modified PFOs results in more closely packed aggregates with the average smallest intermolecular distances of ~3.3 eV, similar to those in PPV aggregates. Note that elimination of the side groups insignificantly changes the torsional disorder in PFO chains; see Figure 5. Because the presence of side chains negligibly changes distributions of torsion angles, we can conclude that the conformational disorder in PCP materials is fairly insensitive to the side alkyl groups. However, side groups have a dramatic effect on the localization properties of electronic orbitals: The PR distribution in modified PFO samples looks similar to those of PPVs aggregates! In amorphous clusters of PFOs without side chains, the highly localized trap states are mostly located near the band edges, while many strongly localized states with PR = 1 appear deep in the CB and VB of PFOs with octyl groups, as compared in Figure 4. Consequently, despite a strong intramolecular disorder, close packing of amorphous polymers results in much better delocalization of molecular orbitals and less probable formation of deep carrier tapping states. This finding can be aligned with experimental measurements of PCP blends, demonstrating that the random incorporation of short and branched alkyl chains increases the efficiency of charge transfer and improves the overall PCP-based solar cell performance.[38]

In summary, our simulations show that the nature of the disorder and its impact on charge-carrier localization in amorphous PFOs and MEH-PPVs with long side chains significantly differ from those without side chains, such as PPV aggregates. We found that the alkyl side chains insignificantly affect the conformational disorder in PCP materials while having a dramatic effect on the intermolecular disorder and packing. Close packing of amorphous PPVs facilitates delocalization of molecular orbitals, while intermolecular disorder results in the formation of localized trap states in the proximity of the band gap. In contrast, long-range intermolecular interactions lead to strong orbital localization and the formation of numerous deep trap states in MEH-PPV and PFO amorphous aggregates. Thus, theoretical methodologies postulating a band-like description for mobility calculations are not appropriate for amorphous PCPs with long side chains.

dx.doi.org/10.1021/jz4003197 | J. Phys. Chem. Lett. 2013, 4, 1453−1459

■ ASSOCIATED CONTENT

Supporting Information

Electronic structure calculations for one of the amorphous samples of MEH-PPV calculated by the "standard" GGA functional PBE, the hybrid functional PBE1, and the long-range corrected functionals LC-ωPBE and comparison of molecular orbitals of two selected MEH-PPV oligomers. This material is available free of charge via the Internet at http://pubs.acs.org.

■ AUTHOR INFORMATION

Corresponding Author

*E-mail: serg@lanl.gov.

Notes

The authors declare no competing financial interest.

■ ACKNOWLEDGMENTS

S.K. thanks ND EPSCoR, NSF Fund EPS-0814442 for partial financial support and the Center for Computationally Assisted Science and Technology (CCAST) at North Dakota State University and the Center for Integrated Nanotechnology (CINT) at Los Alamos National Laboratory for computer access and administrative support. D.L.S and R.L.M. acknowledge the support from the DOE Office of Basic Energy Sciences (OBES) under Work Proposal Number 08SCPE973. S.T., A.S., and E.R.B. acknowledge the support from the US Department of Energy and Los Alamos National Laboratory (LANL) Directed Research and Development Funds. Los Alamos National Laboratory is operated by Los Alamos National Security, LLC, for the National Nuclear Security Administration of the U.S. Department of Energy under contract DE-AC52-06NA25396.

■ REFERENCES

(1) Malliaras, G.; Friend, R. *Phys. Today* **2005**, *58*, 53−58.
(2) Gunes, S.; Neugebauer, H.; Sariciftci, N. *Chem. Rev.* **2007**, *107*, 1324−1338.
(3) Heeger, A. J. *Chem. Soc. Rev.* **2010**, *39*, 2354−2371.
(4) Como, E. D.; Becker, K.; Feldmann, J.; Lupton, J. M. *Nano Lett.* **2007**, *7*, 2993−2998.
(5) Barbara, P. F.; Chang, W. S.; Link, S.; Scholes, G. D.; Yethiraj, A. *Annu. Rev. Phys. Chem.* **2007**, *58*, 565−584.
(6) Tretiak, S.; Saxena, A.; Martin, R. L.; Bishop, A. R. *Phys. Rev. Lett.* **2002**, *89*, 097402.
(7) Thorsmolle, V. K.; Averitt, R. D.; Demsar, J.; Smith, D. L.; Tretiak, S.; Martin, R. L.; Chi, X.; Crone, B. K.; Ramirez, A. P.; Taylor, A. J. *Phys. Rev. Lett.* **2009**, 102.
(8) Hallam, T.; Lee, M.; Zhao, N.; Nandhakumar, I.; Kemerink, M.; Heeney, M.; McCulloch, I.; Sirringhaus, H. *Phys. Rev. Lett.* **2009**, 103.
(9) Guo, J.; Ohkita, H.; Benten, H.; Ito, S. *J. Am. Chem. Soc.* **2009**, *131*, 16869−16880.
(10) Ortmann, F.; Bechstedt, F.; Hannewald, K. *Phys. Status Solidi B* **2011**, *248*, 511−525.
(11) Bolinger, J. C.; Traub, M. C.; Adachi, T.; Barbara, P. F. *Science* **2011**, *331*, 565−567.
(12) Franco, I.; Tretiak, S. *J. Am. Chem. Soc.* **2004**, *126*, 12130−12140.
(13) Coropceanu, V.; Cornil, J.; da Silva Filho, D.; Olivier, Y.; Silbey, R.; Bredas, J.-L. *Chem. Rev.* **2007**, *107*, 926−952.
(14) Nayyar, I. H.; Batista, E. R.; Tretiak, S.; Saxena, A.; Smith, D. L.; Martin, R. L. *J. Phys. Chem. Lett.* **2011**, *2*, 566−571.
(15) Nayyar, I. H.; Batista, E. R.; Tretiak, S.; Saxena, A.; Smith, D. L.; Martin, R. L. *J. Chem. Theory Comput.* **2013**, *9*, 1144−1154.
(16) Tretiak, S.; Igumenshchev, K.; Chernyak, V. *Phys. Rev. B* **2005**, *71*, 33201.
(17) Wu, C.; Tretiak, S.; Chernyak, V. Y. *Chem. Phys. Lett.* **2007**, *433*, 305−311.
(18) Yang, P.; Batista, E. R.; Tretiak, S.; Saxena, A.; Martin, R. L.; Smith, D. L. *Phys. Rev. B* **2007**, *76*, 241201.
(19) Kilina, S.; Batista, E. R.; Yang, P.; Tretiak, S.; Saxena, A.; Martin, R. L.; Smith, D. L. *ACS Nano* **2008**, *2*, 1381−1388.
(20) Granadino-Roldan, J.; Vukmirovic, N.; Fernandez-Gomez, M.; Wang, L.-W. *Phys. Chem. Chem. Phys.* **2011**, *13*, 14501−14510.
(21) Yarotski, D. A.; Kilina, S. V.; Talin, A. A.; Tretiak, S.; Prezhdo, O. V.; Balatsky, A. V.; Taylor, A. J. *Nano Lett.* **2009**, *9*, 12−17.
(22) Kuik, M.; Nicolai, H. T.; Lenes, M.; Wetzelaer, G.-J. A. H.; Lu, M.; Blom, P. W. M. *J. Appl. Phys.* **2011**, *98*, 093301−1−3.
(23) Wetzelaer, G. A. H.; Kuik, M.; Nicolai, H. T.; Blom, P. W. M. *Phys. Rev. B* **2011**, *83*, 165204−1−5.
(24) So, F.; Kondakov, D. *Adv. Mater.* **2010**, *22*, 3762−3777.
(25) Pranaitis, M.; Sakavicius, A.; Janonis, V.; Kazukauskas, V. *J. Appl. Phys.* **2013**, *113*, 013104−1−6.
(26) Ponder, J. W. *TINKER: Software Tools for Molecular Design*, version 3.8; Washington University School of Medicine: Saint Louis, MO, 2000.
(27) Kresse, G.; Furtmüller, J. *Phys. Rev. B* **1996**, *54*, 11169.
(28) Vanderbilt, D. *Phys. Rev. B* **1990**, *41*, 7892.
(29) Perdew, J. P. In *Electronic Structure of Solids*; Ziesche, P., Eschrig;, H., Eds.; Akademie Verlag: Berlin, 1991.
(30) Frisch, M. J.; et al. *Gaussian 09*, revision A.01.; Gaussian, Inc.: Wallingford, CT, 2009.
(31) Abtew, T.; Drabold, D. *Phys. Rev. B* **2006**, *74*, 085201.
(32) Edwards, J. T.; Thouless, D. J. *J. Phys. C: Solid State Phys.* **1972**, *5*, 807.
(33) Bell, R. J.; Dean, P.; Hibbins-Butler, D. C. *J. Phys. C: Solid State Phys.* **1970**, *4*, 1214.
(34) Ono, Y.; Ohtsuki, T.; Kramer, B. *J. Phys. Soc. Jpn.* **1989**, *58*, 1705−1716.
(35) Kuik, M.; Vandenbergh, J.; Goris, L.; Begemann, E. J.; Lutsen, L.; Vanderzande, D. J. M.; Manca, J. V.; Blom, P. W. M. *J. Appl. Phys.* **2011**, *99*, 183305−1−3.
(36) Becker, K.; Como, E. D.; Feldmann, J.; Scheliga, F.; Csanyi, E. T.; Tretiak, S.; Lupton, J. M. *J. Phys. Chem. B* **2008**, *112*, 4859−4864.
(37) Clark, J.; Nelson, T.; Tretiak, S.; Cirmi, G.; Lanzani, G. *Nat. Phys.* **2012**, *8*, 225−231.
(38) Burkhart, B.; Khlyabich, P. P.; Thompson, B. C. *Macromolecules* **2012**, *45*, 3740−3748.